

Extended tunnelling states in the benzoic acid crystal: Infrared and Raman spectra of the OH and OD stretching modes†

François Fillaux, François Romain, Marie-Hélène Limage and Nadine Leygue

Received 27th June 2006, Accepted 9th August 2006

First published as an Advance Article on the web 18th August 2006

DOI: 10.1039/b609078h

We compare Raman and infrared spectra of the ν OH/OD modes in benzoic acid crystal powders at 7 K. The extremely sharp Raman bands contrast to the broad infrared profiles and suggest adiabatic separation of hydrogen (deuterium) dynamics from the crystal lattice. There is no evidence of any proton–proton coupling term. The assignment scheme is consistent with a quasisymmetric double-minimum potential, largely temperature independent. Tunnel splitting is a major band shaping mechanism, in addition to anharmonic coupling with lattice modes. The proton/deuteron dynamics are rationalized with nonlocal pseudoparticles and extended states. We propose a symmetry-related damping mechanism to account for the broad infrared profiles, as opposed to the sharp Raman bands. We assign spectral features to distinct interconversion mechanisms based on either pseudoparticle transfer or adiabatic pairwise transfer. We establish close contacts with theoretical models based on first-principles calculations.

1. Introduction

Proton transfer across hydrogen bonds is of fundamental importance to many physical, chemical and biophysical processes.^{1–7} There is a general agreement that dynamics can be modelled as light particles moving along local reaction coordinates coupled to the motion of heavy atoms. These dynamics are dominated by strong quantum effects with pronounced sensitivity to isotope substitution.

In the crystalline state, the benzoic acid (C_6H_5COOH) form centrosymmetric dimers linked by moderately strong hydrogen bonds. Single-crystal neutron diffraction studies show that protons are largely ordered at low temperatures in the same crystallographic configuration (say **T1** in Fig. 1). As the temperature is increased, protons are progressively transferred to **T2** and the population degrees are almost equal at room temperature.⁸ This thermally activated interconversion, or tautomerism, is monitored by proton transfer dynamics.

NMR^{9–12} and quasi-elastic neutron scattering (QENS)¹³ have confirmed that **T1** and **T2** are quasi-degenerate. The proton transfer rate varies from $\sim 10^8$ to 10^{11} s⁻¹ between 10 and 300 K. The non-vanishing rate at low temperature suggests phonon-assisted tunnelling.¹⁴ The interconversion mechanism was at first modelled as a stochastic single-step pairwise proton transfer, through-barrier tunnelling at low temperature and over-barrier jumping at elevated temperatures.

At the time-scale of 10^{-12} – 10^{-14} s probed with vibrational spectroscopy (infrared, Raman, and inelastic neutron scattering-INS), it is possible to distinguish two competing mechan-

isms.¹⁵ Firstly, coherent phonon-assisted tautomerism prevailing at low temperatures. Secondly, uncorrelated transfer of bare protons in a quasi-symmetrical double minimum potential with a high barrier leading to a two-step tunnelling process at elevated temperatures. On the time-scale of 10^{-6} – 10^{-11} s probed with NMR and QENS the time-averaged two-step interconversion is apparently consistent with a single-step pairwise mechanism.

The double minimum potential for bare protons has been questioned by calculations carried out with advanced quantum chemistry methods^{16–20} and NMR experiments.²¹ We present below further investigations of the infrared and Raman spectra of the OH/OD stretching modes of benzoic acid, a follow up of a previous work.¹⁵ The motivation was twofold: (i) to unravel the band-shaping mechanisms for the ν OH/OD spectral profiles and (ii) to reach a deeper view of quantum dynamics for proton transfer.

A key information to determine the double minimum potential is the tunnel splitting of the ν OH/OD bands. In the infrared and Raman spectra, this splitting is embedded in a series of band shaping mechanisms such as: strong coupling with low frequency modes; fast relaxation; Davydov ($u - g$) splitting; Fermi or multiphonon resonances; hot bands; electrical anharmonicity; breakdown of the selection rules.^{3,18,22} It is therefore difficult, if not impossible, to establish unquestionable assignment schemes.

Some of these mechanisms yield noticeable differences in the infrared and Raman spectra and can be therefore distinguished (for example, $u-g$ splitting, electrical anharmonicity,

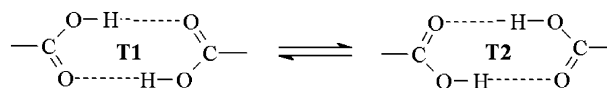


Fig. 1 Sketch of the tautomeric equilibrium in centrosymmetric hydrogen bonded dimers.

LADIR-CNRS, UMR 7075 Université Pierre et Marie Curie, 2 rue Henry Dunant, 94320 Thiais, France. E-mail: fillaux@glvt-cnrs.fr
<http://ulysse.glvt-cnrs.fr/ladir/pagefillaux.htm>

† The HTML version of this article has been enhanced with additional colour images.

selection rules). However, whereas there are published works on the infrared profiles of benzoic acid,^{15,18,23} the Raman spectra have been seemingly overlooked. The prevailing idea is that the $\nu\text{OH}/\text{OD}$ bands should be broad and too weak to be confidently measured. In marked contrast to this prejudice, we show below that these bands are extremely sharp and clearly visible. Consequently, some dubious assignments in the infrared are straightforward in Raman and lead to the conclusion that the double minimum potential itself is a major band shaping mechanism. Thus, we can determine the effective potentials for proton/deuteron transfer and correlate the observed eigen states with interconversion energetics.

The dynamical model presented below is largely inspired by a work on potassium hydrogen carbonate (KHCO_3),²⁴ another system composed of centrosymmetric hydrogen bonded dimers (HCO_3^-)₂. Accordingly, we shall introduce nonlocal pseudoparticles and macroscopic tunnelling states. However, it should be emphasized from the very beginning that the interpretation of the Raman spectra presented below is discouragingly difficult and it is unrealistic to pretend that any reasonable assignment scheme, necessarily tentative, can prove (or disprove) any model in its own right. The purpose is more modestly to establish whether spectra are not inconsistent with the preferred model, already based on totally independent experiments and plausible theoretical background.

In section 2, we compare the infrared and Raman $\nu\text{OH}/\text{OD}$ profiles of three isotope derivatives of benzoic acid at 7 K: the fully hydrogenated ($\text{BA-}h_6$); the ring-deuterated ($\text{BA-}d_5h$); the O-deuterated ($\text{BA-}h_5d$). We also report spectra of $\text{BA-}d_5h$ at various temperatures up to 300 K. In section 3, we propose an assignment scheme and we determine the double-minimum potential functions for the stretching modes. In section 4, we elaborate a purely quantum mechanical model based on nonlocal pseudoparticles and extended tunnelling states. We show that “zero-phonon” transitions can be related to the pairwise transfer. Finally, we show that potential functions derived from vibrational spectra are in excellent agreement with those calculated with first-principles methods. Experimental details are given in section 5.

2. Infrared and Raman spectra

The benzoic acid crystal is monoclinic at any temperature up to 300 K. The space group is $P2_1/c$ (C_{2h}^5) with 4 crystallographically equivalent $\text{C}_6\text{H}_5\text{COOH}$ entities in the unit cell forming nearly planar centrosymmetric dimers (C_i) linked by hydrogen bonds of length $R_{\text{O}\cdots\text{O}} \approx 2.61 \text{ \AA}$ at 20 K.^{8,25}

There are 177 vibrational modes that can be decomposed into 156 internal and 21 external vibrations.²³ A full assignment scheme would require theoretical modelling, beyond the scope of the present work. Our purpose is therefore limited to assigning νOH and νCH bands on the basis of isotope frequency shifts.

The intense νCH Raman bands of $\text{BA-}h_6$ are observed between 3000 and 3200 cm^{-1} (Fig. 2). For $\text{BA-}d_5h$, the νCD 's are at 2250–2300 cm^{-1} (Fig. 3). The very weak decoupled CH bonds due to traces of undeuterated aromatic sites ($\approx 2\%$) peak at 3073 cm^{-1} . The band at 3168 and the shoulder at 3210 cm^{-1} ($\text{BA-}h_6$) are unaffected by O-deuteration ($\text{BA-}h_5d$, Fig. 4)

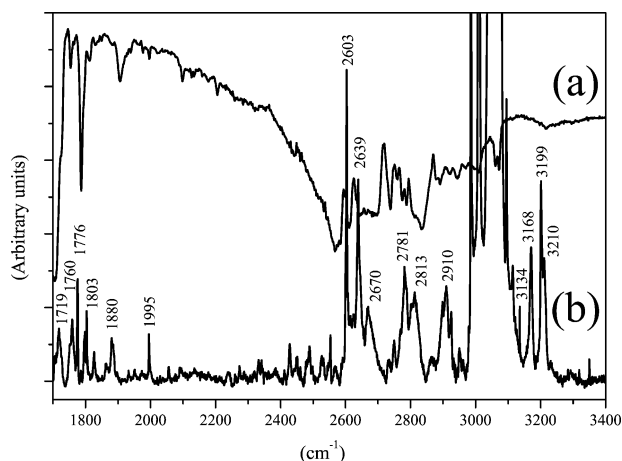


Fig. 2 Comparison of the spectral profiles for crystal powders of the fully hydrogenated benzoic acid at 7 K. (a) Infrared transmittance. (b) Raman intensity. Numbers are Raman frequency shifts.

and disappear upon ring deuteration ($\text{BA-}d_5h$, Fig. 3). They can be assigned to CH-containing modes.

The most intense Raman bands between 2600 and 2950 cm^{-1} have a pronounced νOH character. The spectra of $\text{BA-}h_5d$ presented in Fig. 4 show the residual νOH bands corresponding to protons ($\approx 15\%$) surrounded by deuterium atoms. The bands labelled with stars (*) are barely visible in Fig. 2, aside the νOH bands. They are not due to traces of OH groups. Presumably, they are overtones and combinations, but a more specific assignment is not possible.

Bands between 2600 and 2675 cm^{-1} are virtually unaffected by ring deuteration and can be therefore attributed to pure νOH . Bands between 2700 and 2950 cm^{-1} in Fig. 2 are also dominantly νOH , although small frequency shifts by a few cm^{-1} upon ring deuteration (compare Fig. 2 and 3) suggest that weak interaction with CH-containing modes should not be totally excluded.

For $\text{BA-}d_5h$ (Fig. 3) the bands at 3134, 3193 and 3260 cm^{-1} are free of CH modes and can be logically attributed to νOH

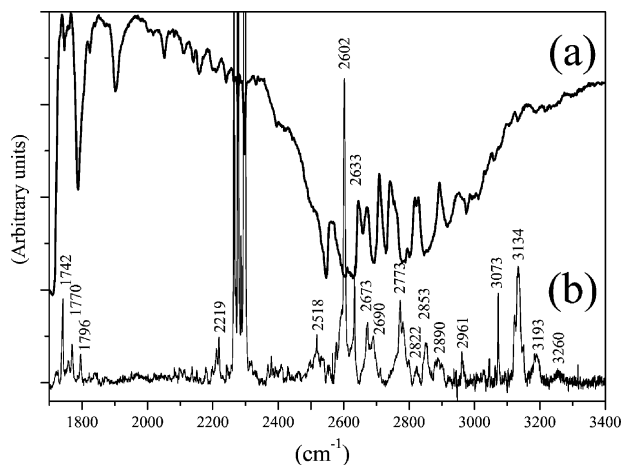


Fig. 3 Comparison of the spectral profiles for crystal powders of the ring-deuterated benzoic acid at 7 K. (a) Infrared transmittance. (b) Raman intensity. Numbers are Raman frequency shifts.

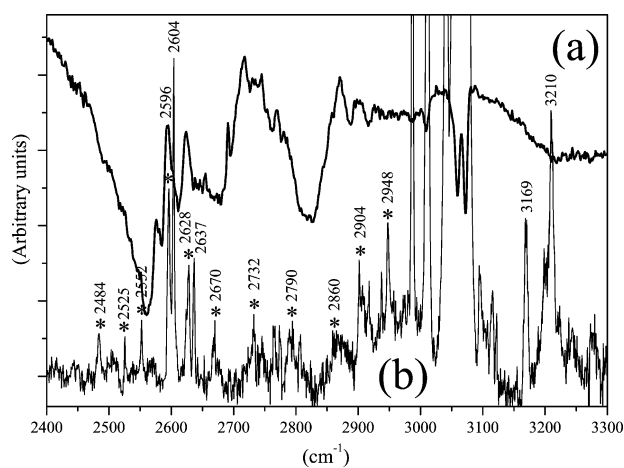


Fig. 4 Comparison of the spectral profiles of traces of OH species ($\leq 15\%$) in the O-deuterated benzoic acid crystal at 7 K. (a) Infrared transmittance. (b) Raman intensity. Numbers are Raman frequency shifts. *: OH-free Raman bands.

modes. For BA- h_6 in Fig. 2, these OH bands are partially superposed to the CH-containing bands at 3168 and 3210 cm^{-1} .

The full width at half maximum (FWHM) of $\approx 5 \text{ cm}^{-1}$ for the main νOH bands at $\approx 2600 \text{ cm}^{-1}$ is in dramatic contrast with the broad infrared profiles. The Raman width is similar to that of the decoupled νCH bands of BA- d_{5h} and close to the spectrometer resolution. (The intrinsic width could therefore be less than observed.) Similar sharp bands were reported for dimers of gaseous formic acid.²⁶ They were assigned to overtones or combinations of internal modes, whereas the stretching profile was attributed to a weak underlying continuum with a breadth of $\approx 400 \text{ cm}^{-1}$. For benzoic acid a similar assignment scheme is untenable. First, there is no convincing evidence of a broad continuum of intensity analogous to that observed in the infrared. Second, combinations are unlikely since all internal modes are shifted by more than 10 cm^{-1} upon ring deuteration and they are much broader than the OH bands at $\approx 2600 \text{ cm}^{-1}$.¹⁵ Third, infrared transmittance windows, possibly due to multiphonon transitions, show more pronounced frequency shifts than the Raman bands and there is no apparent correlation between the spectra. The sharp bands are therefore confidently attributed to νOH modes.

For BA- h_{5d} in Fig. 5, Raman νOD bands at 2041 and 2198 cm^{-1} are at nearly the same frequencies as infrared bands at 2052 and 2202 cm^{-1} , and relative intensities are comparable. Here again, Raman bands are much narrower (FWHM $\approx 7 \text{ cm}^{-1}$) than their infrared counterparts (FWHM ≈ 40 and 80 cm^{-1} , respectively), although with less marked contrast than for νOH bands.

In Fig. 4, the residual νOH bands correspond essentially to mixed HD dimers ($\approx 30\%$), whereas HH pairs ($\approx 2\%$) can be ignored. Visual comparison with Fig. 2 shows that νOH bands are neither shifted, nor broadened, by statistical surroundings of deuterons. Clearly, intra- and inter-dimer coupling terms are rigorously negligible. This is at variance with theoretical estimates of the Davydov splitting, up to $\approx 100\text{--}200 \text{ cm}^{-1}$.^{17,18}

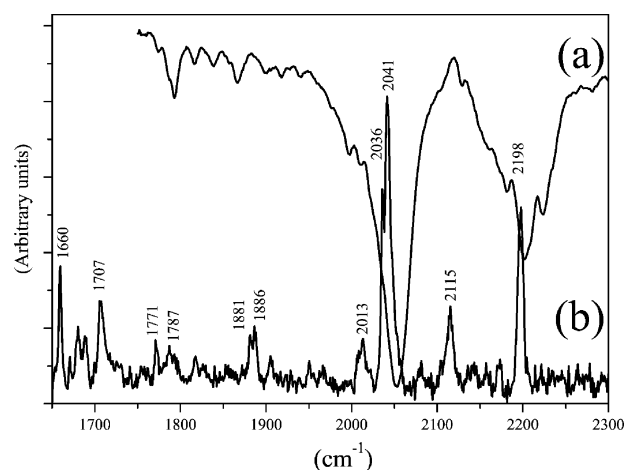


Fig. 5 Comparison of the spectral profiles for crystal powders of the O-deuterated benzoic acid at 7 K. (a) Infrared transmittance. (b) Raman intensity. Numbers are Raman frequency shifts.

Fermi resonance is widely recognized as an important band shaping mechanism. Such anharmonic coupling with multiphonons can be modelled as coupled multi-level systems. However, Raman bands are so narrow that resonance should be more seldom seen than in the infrared. In addition, since $\nu\text{OH}/\text{OD}$ band intensities are extremely weak, multiphonon transitions may appear even if there is no resonance. For example, weak bands between 2200 and 2600 cm^{-1} in Fig. 2 and 3 could be multiphonons. Similarly, some bands in the 1700–2000 cm^{-1} range (Fig. 2) disappear upon ring deuteration (Fig. 3) and some others are shifted downward for BA- h_{5d} (Fig. 5). There are probably multiphonons as well as $\nu\text{OH}/\text{OD}$ bands analogous to the intense infrared bands in the same range. In any case, the very large number of internal modes hampers a precise assignment scheme.

By contrast to Raman, anharmonic coupling of the infrared continuum with narrow multiphonons may yield transmittance windows^{27,28} or even more complicated profiles.²⁹ For example, among the Raman bands at 2822, 2853, and 2890 cm^{-1} (Fig. 3), the central component could be νOH , for it corresponds to a minimum of the infrared transmittance, while the two side-bands corresponding to transmittance windows could be multiphonons. However, this rule of thumb should be used with caution. For example, νOH bands at 2603 and 2639 cm^{-1} in BA- h_6 (Fig. 2) are close to infrared transmission windows, while their analogues in Fig. 3 do not correspond to such windows. In fact, the isotope mixture in Fig. 4 enhances multiphonon bands at 2596 and 2628 cm^{-1} , corresponding to the transmission windows, which were not resolved in the fully hydrogenated derivative. Presumably, these bands and their transmission windows are shifted downward upon ring deuteration, while the νOH is little affected.

Raman spectra at various temperatures (Fig. 6), in line with infrared spectra,¹⁵ do not provide conclusive evidence for any significant change of proton dynamics. The νOH bands are marginally broadened at 300 K, frequencies are almost unaffected and the overall profile is little changed. The potential function for protons is therefore largely temperature independent. This is remarkable since between 7 and 300 K protons

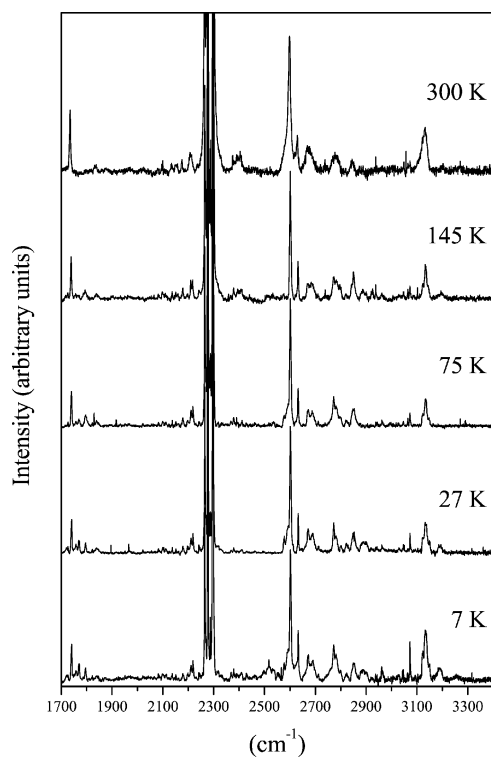


Fig. 6 Raman spectral profiles for a crystal powder of the ring-deuterated benzoic acid at various temperatures.

are progressively transferred to unoccupied sites⁸ and there are spectacular changes of the lattice modes at low frequency.¹⁵ Clearly, there is no evidence for stochastic disorder, or any transition from the quantal to the classical regime. This is in marked contrast with conclusions presented in other works.^{14,20,30,31}

3. Proton dynamics

In this section, Raman spectra are tentatively rationalized with the dynamical model proposed in ref. 15. This model is based on three features of moderately strong OH \cdots O hydrogen bonds. First, the stretching mode experiences a quasi-symmetrical double minimum potential (see Fig. 13 in ref. 15). In contrast to the symmetric case, energy levels have no particular symmetry and can be labelled in order of their increasing energy, $n = 0, 1, 2, 3, \dots$. The ground-state splitting has been measured with INS for BA-*d*₅h ($|0\rangle \leftrightarrow |1\rangle \approx 172 \text{ cm}^{-1}$) and upper states were derived from infrared profiles ($|0\rangle \leftrightarrow |2\rangle \approx 2570 \text{ cm}^{-1}$ and $|0\rangle \leftrightarrow |3\rangle \approx 2840 \text{ cm}^{-1}$). The ground state splitting, largely dominated by the potential asymmetry, should not be confused with tunnelling. For the symmetrized potential the estimated tunnel splitting is $h\nu_{0t} \approx 6 \text{ cm}^{-1}$.

Within the two-level system approximation,^{15,32} wave functions for the $|0\rangle$ and $|1\rangle$ levels can be written as:

$$\begin{aligned} \Psi_0 &= \cos \phi \psi_0(x - x_0) + \sin \phi \psi_0(x + x_0) \\ \Psi_1 &= -\sin \phi \psi_0(x - x_0) + \cos \phi \psi_0(x + x_0) \end{aligned} \quad (1)$$

The harmonic wave functions $\psi_0(x - x_0)$ and $\psi_0(x + x_0)$ are eigen functions of the Hamiltonian obtained by second-order

expansion of the potential around the minima at $\pm x_0$. Then, $\tan 2\phi = \nu_{0t}/(\nu_{01} - \nu_{0t})$ gives: $\cos \phi \approx 1$ and $\sin \phi = \varepsilon \approx 1.8 \times 10^{-2}$.¹⁵ The delocalization degree of the wave function (ε) measures the degree of symmetry for the double well: $\varepsilon^2 = 1/2$ in the symmetric case and $\varepsilon = 0$ for the totally asymmetric potential. By definition, the potential is quasi-symmetric for $0 < \varepsilon^2 < 1/2$. The key parameter ε determines the intensity of the $0 \leftrightarrow 1$ transition. This transition has never been observed with infrared and Raman, presumably because it is too weak to emerge from other bands in the same range (for example $\nu\text{O}\cdots\text{O}$). However, it was observed with INS, thanks to the large incoherent scattering cross-section of protons.

The second feature is the adiabatic separation of the proton/deuteron dynamics from heavy atoms. Raman band-widths emphasize very long lifetimes for $\nu\text{OH}/\text{OD}$ excited states, on the time-scale of heavy atom dynamics. Any relaxation mechanism, in particular nonadiabatic terms,²² can be safely ignored. The νOH dynamics is therefore amenable to bare protons/deuterons and non-crossing adiabatic potentials for heavy atoms. As the nonadiabatic coupling terms do not depend on the spectroscopy technique, the very broad infrared profiles suggest homogeneous broadening by a very fast relaxation mechanism of a different origin. We suggest below a symmetry-related damping mechanism (holding for u modes in the infrared but not for g species in Raman) specific to double minimum potentials.

The third feature is the strong coupling between $\nu\text{OH}/\text{OD}$ and $R_{\text{O}\cdots\text{O}}$ distances.³³ Since the seminal paper by Stepanov,³⁴ strong coupling and adiabatic separation are cornerstones of the dynamical models for moderately strong hydrogen bonds.^{3,15,22,35–38} The minimum of the adiabatic potential for $\nu\text{O}\cdots\text{O}$ in $\nu\text{OH}/\text{OD}$ excited states is shifted toward short $R_{\text{O}\cdots\text{O}}$ distances, in the range characteristic of short symmetric hydrogen bonds. Simultaneously, the $\nu\text{O}\cdots\text{O}$ frequency increases and the νOH decreases, both dramatically.

In Fig. 7, the upper adiabatic potentials are semi-quantitatively sketched with Morse functions. We label $|n_{\text{OH}}\rangle_{g/u}$ $|N_{\text{OO}}\rangle_{ng/lu}$ the state vectors in the n th $\nu_{g/u}$ OH and N th $\nu\text{O}\cdots\text{O}$ state. Transitions from the ground state $|0_{\text{OH}}\rangle_{g/u}|0_{\text{OO}}\rangle_{0g}$ give Franck–Condon-like progression bands whose relative intensities depend on the overlap integral for the wave functions along ΔR . The most intense bands correspond to “ N -phonons” vertical transitions ($\Delta N_{\text{OO}} \geq 1$) while the “zero-phonon” transitions ($\Delta N_{\text{OO}} = 0$) are much weaker.^{3,37} Note that infrared-active zero-phonon transitions, namely $|0_{\text{OH}}\rangle_{u}|0_{\text{OO}}\rangle_{0u} \leftrightarrow |2_{\text{OH}}\rangle_{u}|0_{\text{OO}}\rangle_{2u}$ and $|0_{\text{OH}}\rangle_{u}|0_{\text{OO}}\rangle_{0u} \leftrightarrow |3_{\text{OH}}\rangle_{u}|0_{\text{OO}}\rangle_{3u}$, are at 1787 and 1907 cm^{-1} , respectively, for BA-*h*₆, 1788 and 1902 cm^{-1} , respectively, for BA-*d*₅h.¹⁵ In contrast to the broad profiles observed for higher transitions, the zero-phonon bands are quite sharp at low temperature. These long-life states are virtually stationary.

It should be needless to emphasize that Fig. 7 is oversimplified. There may be additional coupling between νOH and low frequency modes, other than $\nu\text{O}\cdots\text{O}$. In addition, overtones and combinations can interact with OH states through anharmonic coupling terms (for example, Fermi resonance).

For OD derivatives, the overall sketch is similar but the upper adiabatic potentials are flattened and the potential slope

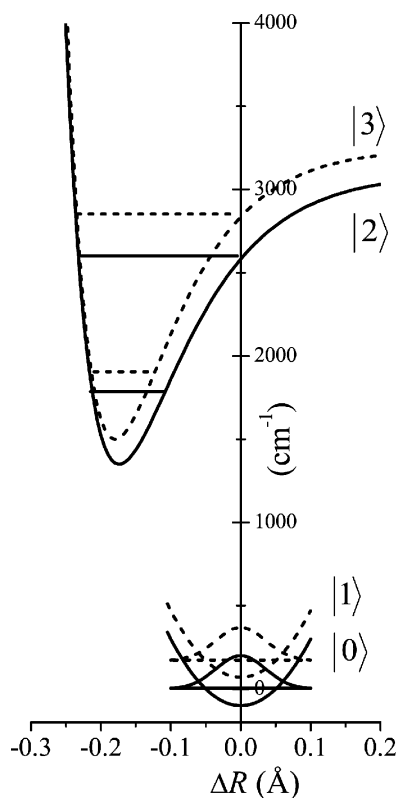


Fig. 7 Schematic view of the effective adiabatic potentials along the $\nu\text{O}\cdots\text{O}$ coordinate ΔR for the νOH states in a quasisymmetric double minimum potential function.

in the relevant ΔR range is decreased. In principle, the minima of the upper states, and therefore the zero-phonon states, are little affected by deuteration.

3.1. Assignment scheme

We assign the most intense νOH Raman bands at about 2600 cm^{-1} to $|0_{\text{OH}}\rangle_g|0_{\text{OO}}\rangle_{0g} \leftrightarrow |2_{\text{OH}}\rangle_g|1_{\text{OO}}\rangle_{2g}$. A previous estimate of 2570 cm^{-1} from infrared profiles¹⁵ was much less accurate since energy levels were poorly defined. As there is no intradimer coupling, the difference between infrared and Raman is not significant.

In Fig. 2, the bands at 2603 , 2639 and 2670 cm^{-1} suggest a Franck–Condon-like progression of the νOH involving a low-frequency mode $\hbar\Omega_1 \approx 33\text{ cm}^{-1}$. A similar pattern is observed in Fig. 3 at 2602 , 2633 and 2673 cm^{-1} ($\hbar\Omega_1' = 35\text{ cm}^{-1}$). Intensity ratios suggest a rather modest coupling, possibly with the lattice mode reported at $\approx 35\text{ cm}^{-1}$.¹⁵ A linear coupling term could slightly shift the equilibrium position along the relevant lattice coordinate in the excited state while leaving the frequency virtually unchanged.

The νOH bands at 2781 and 2813 cm^{-1} (Fig. 2) could be combinations of those at 2603 and 2639 cm^{-1} with $\hbar\Omega_2 = 178\text{ cm}^{-1}$. Similarly, the sharp νOH band at 2773 cm^{-1} for BA-*d*₅*h* (Fig. 3) could be a combination of that at 2602 cm^{-1} with $\hbar\Omega_2' \approx 171\text{ cm}^{-1}$. However, for both systems, $\hbar\Omega_2$ and $\hbar\Omega_2'$ are quite different from the observed lattice frequencies, for instance at 199.0 , 133.5 cm^{-1} for BA-*h*₆, or 189.5 , 129.5

Table 1 Energy levels in cm^{-1} units derived from $\nu\text{OH}/\text{OD}$ Raman bands

	$ 2\rangle_g 1_{\text{OO}}\rangle_{2g}$	$ 2\rangle_g 1_{\text{OO}}\rangle_{2g} + 1\rangle_g 0_{\text{OO}}\rangle_{1g}$	$ 3\rangle_g 1_{\text{OO}}\rangle_{3g}$
BA- <i>h</i> ₆	2603	2781	2910
BA- <i>d</i> ₅ <i>h</i>	2602	2773	2853
BA- <i>h</i> ₅ <i>d</i>	2041	2198	—

cm^{-1} for BA-*d*₅*h*.¹⁵ Although strong nonlinear coupling terms cannot be excluded for sure, it is possible to assign the BA-*d*₅*h* band at 2773 cm^{-1} to a combination with the $|0\rangle \leftrightarrow |1\rangle$ transition previously observed at 172 cm^{-1} .¹⁵ Although the analogue transition for the fully hydrogenated derivative is unknown, it is not unrealistic to suppose, for the sake of consistency, that the $|0\rangle \leftrightarrow |1\rangle$ splitting is shifted to $\approx 178\text{ cm}^{-1}$ for that derivative (Table 1).

For the νOH band of BA-*h*₆ at 2910 cm^{-1} , the frequency shift to 2853 cm^{-1} upon ring-deuteration is much greater than anticipated for any combination with lattice or internal modes. In accordance with infrared spectra, these bands are assigned to transitions to the upper νOH state: $|0_{\text{OH}}\rangle_g|0_{\text{OO}}\rangle_{0g} \leftrightarrow |3_{\text{OH}}\rangle_g|1_{\text{OO}}\rangle_{3g}$. The bands at 3134 , 3193 and 3260 cm^{-1} for BA-*d*₅*h* are tentatively attributed to further Franck–Condon-like transitions to upper $\nu\text{O}\cdots\text{O}$ states: $|0_{\text{OH}}\rangle_g|0_{\text{OO}}\rangle_{0g} \leftrightarrow |2_{\text{OH}}\rangle_g|2_{\text{OO}}\rangle_{2g}$ and $|3_{\text{OH}}\rangle_g|2_{\text{OO}}\rangle_{3g}$. These states are probably close to the upper potential thresholds.

For BA-*h*₅*d* (Fig. 5), we assign the νOD Raman bands at 2041 and 2198 cm^{-1} by analogy with the νOH (Table 1). Then, the ground state splitting should be 157 cm^{-1} . However, there is no distinct band to be assigned to the upper νOD state $|3_{\text{OD}}\rangle_g|1_{\text{OO}}\rangle_{3g}$ (see below, section 3.2) and there is no clear interpretation for the weak bands around 1880 , 2013 and 2115 cm^{-1} , which could be multiphonons.

Finally, some Raman bands of the OH derivatives in the 1700 – 1800 cm^{-1} region should be the analogues of the infrared active zero-phonon transitions. However, there are also multiphonon bands and it is not possible to propose a precise assignment scheme. For BA-*h*₅*d*, nevertheless, there is no objection to attribute the main peaks at 1660 and 1707 cm^{-1} to zero-phonons: $|0_{\text{OD}}\rangle_g|0_{\text{OO}}\rangle_{0g} \leftrightarrow |2_{\text{OD}}\rangle_g|0_{\text{OO}}\rangle_{2g}$ and $|0_{\text{OD}}\rangle_g|0_{\text{OO}}\rangle_{0g} \leftrightarrow |3_{\text{OD}}\rangle_g|1_{\text{OO}}\rangle_{3g}$, respectively, although these transitions cannot be confirmed in the infrared as they are hidden by intense νCO bands.¹⁵

3.2. Double minimum potentials

The assignment scheme in Table 1 leads to the conclusion that Raman spectra allow us to determine the ground state splitting that cannot be measured otherwise, except with INS for the ring deuterated derivative. The effective double minimum potentials in Table 2 were determined through best fit exercises.¹⁵ Since there are only three energy levels and four parameters, we have included relative intensities as further constraints. In addition, distances between minima Δr were kept in reasonable agreement with neutron diffraction data. Needless to say, alternative mathematical functions could be envisaged but they would yield similar potential shapes.

For a given set of energy levels and relative intensities, Δr depends on the effective oscillator mass that is therefore an

Table 2 Potential functions, energy levels, and potential barriers (H) in cm^{-1} units derived from the assignment schemes presented in Table 1. The tunnel splitting of the symmetrized potential function is $h\nu_{0t}$. The distances between minima (Δr) and x are in \AA units

	V	Δr	H	$h\nu_{0t}$	$h\nu_{01}$	$h\nu_{02}$	$h\nu_{03}$
BA- h_6	$281x + 301370x^2 + 172300 \exp(-2.27x^2)$	0.68	4990	7.7	178	2603	2910
BA- d_{sh}	$270x + 282880x^2 + 171120 \exp(-2.15x^2)$	0.69	5006	6.0	171	2602	2853
BA- h_{5d}	$240x + 299010x^2 + 171980 \exp(-2.265x^2)$	0.68	4488	0.2	156	2041	2181

adjustable parameter. Within the experimental accuracy for Δr , the effective mass is 1 (2) amu for OH (OD) derivatives, and the potential coordinate is along the straight line joining the minima. Greater masses would give unrealistic shorter Δr 's.

The barrier decreases substantially upon O-deuteration while the effect of ring deuteration is tiny (Table 2). A similar decrease upon OH/OD substitution was reported for potassium hydrogen/deuterium carbonate.³⁸ If the potentials were mere cuts of the Born–Oppenheimer surface along classical trajectories, they should be unaffected by H/D substitution. Alternatively, the observed eigenstates define “effective” potentials depending on the domains spanned by the zero-point motions of H or D atoms. This effect is important for OH/OD substitution and tiny for ring deuteration.

The tunnelling frequency $h\nu_{0t}$ decreases substantially for the OD derivative, in spite of the lower barrier. The states are quite localized in their respective wells and the intensity of $|0_{\text{OD}}\rangle \leftrightarrow |3_{\text{OD}}\rangle$ is depressed. In addition, this transition is calculated at about the same frequency as $[|0_{\text{OD}}\rangle \leftrightarrow |2_{\text{OD}}\rangle] + [|0_{\text{OD}}\rangle \leftrightarrow |1_{\text{OD}}\rangle]$, thanks to the weak tunnel splitting for the upper states ($\approx 15 \text{ cm}^{-1}$ for the symmetrized potential). Therefore, the Raman band at 2198 cm^{-1} in Fig. 5, as well as its infrared counterpart, are likely to be unresolved superpositions of the two transitions.

4. Discussion

It may seem straightforward to suppose that the double-well potential should monitor uncorrelated transfer of bare protons or deuterons.¹⁵ However, this interpretation is refuted by two counterarguments. Firstly, the energy cost for conversion into dimers composed of “biprotinated” and “deprotinated” entities should be much greater than $h\nu_{01}$. Secondly, the center of symmetry should be destroyed at elevated temperatures and the g – u selection rules for internal modes should be cancelled. On the contrary, there is no evidence for symmetry breaking at any time-scale (neutron diffraction⁸ or spectroscopy¹⁵). Consequently, we have to conceive a dynamical model preserving the center of symmetry. We present below a simplified version of a theory elaborated for KHCO_3 and presented in details in ref. 24,39. See also ref. 40 for isolated dimers in the gas phase.

4.1. Pseudoparticle dynamics

Within the adiabatic separation, the stretching modes of a dimer are modelled with two collinear harmonic oscillators x_1 and x_2 , each with mass m . The centrosymmetric normal coordinates and conjugated momenta

$$\begin{aligned} x_g &= \frac{1}{\sqrt{2}}(x_1 - x_2), & P_g &= \frac{1}{\sqrt{2}}(P_1 - P_2), \\ x_u &= \frac{1}{\sqrt{2}}(x_1 + x_2), & P_u &= \frac{1}{\sqrt{2}}(P_1 + P_2), \end{aligned} \quad (2)$$

split the coupled oscillators into uncoupled normal modes. These normal coordinates are independent of the coupling strength between oscillators (too weak to be observed in the present case). They are dictated by the crystal structure.

In quantum mechanics, normal modes define pseudoparticles \mathcal{P}_g and \mathcal{P}_u , each with mass $m = 1$ (H) or 2 (D) amu, corresponding to symmetric or antisymmetric displacements of two “half-pseudoparticles”. These pseudoprotons are observables and their mass is dictated by experiments. They are nonlocal since individual positions and momenta of the “real” particles (x_1, P_1 and x_2, P_2) are not observables.

Pseudoparticles offer a graphical representation of dynamics in double wells (Fig. 8). In the ground state, \mathcal{P}_g and \mathcal{P}_u are superposed in configuration **T1** (grey circles), to order ϵ . In excited states, wave functions are largely delocalized over the two wells (see Fig. 13 in ref. 15) and displacement vectors acquire very large amplitudes ($\approx \Delta r$). Raman active transitions can be thought of as symmetric excitations of the two half-pseudoparticles of \mathcal{P}_g to upper delocalized states. In fact, transitions involving \mathcal{P}_u are also Raman active because the u symmetry for small oscillations with respect to the equilibrium configuration is superseded by large symmetric displacements in the excited state. The upper states can be thus written as: $|2g/u\rangle|0u/g\rangle|1_{\text{OO}}\rangle_{2g/u}|0_{\text{OO}}\rangle_{0u/g}$, or $|3g/u\rangle|0u/g\rangle|1_{\text{OO}}\rangle_{3g/u}|0_{\text{OO}}\rangle_{0u/g}$ (Fig. 8 g) and the combination states for simultaneous excitations of \mathcal{P}_g and \mathcal{P}_u as: $|2g/u\rangle|1u/g\rangle|1_{\text{OO}}\rangle_{2g/u}|0_{\text{OO}}\rangle_{1u/g}$.

In order to sustain this assignment scheme, we can estimate Raman intensities. They are proportional to

$$\begin{aligned} \mathcal{I}_{00 \leftrightarrow 20} &= |\langle 2g | \langle 0u | \langle 1_{\text{OO}} |_{2g} \langle 0_{\text{OO}} |_{0u} [x] | 0g \rangle | 0u \rangle | 0_{\text{OO}} \rangle_{0g} | 0_{\text{OO}} \rangle_{0u} |^2 \rangle \\ \mathcal{I}_{00 \leftrightarrow 21} &= |\langle 2g | \langle 1u | \langle 1_{\text{OO}} |_{2g} \langle 0_{\text{OO}} |_{1u} [x] | 0g \rangle | 0u \rangle | 0_{\text{OO}} \rangle_{0g} | 0_{\text{OO}} \rangle_{0u} |^2 \rangle \end{aligned} \quad (3)$$

In addition, $\mathcal{I}_{00 \leftrightarrow 02} = \mathcal{I}_{00 \leftrightarrow 20}$, $\mathcal{I}_{00 \leftrightarrow 12} = \mathcal{I}_{00 \leftrightarrow 21}$. Intensities depend on the transition moment for νOH multiplied by the overlap integral for $\nu\text{O} \cdots \text{O}$. We limit the expansion of the polarizability tensor to first order as $[x] = [x]_1 x$. Numerical integration of the transition moment for νOH gives $\mathcal{I}_{00 \leftrightarrow 02} / \mathcal{I}_{00 \leftrightarrow 12} \approx 25$. On the other hand the overlap integral $|\langle 0_{\text{OO}} |_{1u/g} \langle 0_{\text{OO}} \rangle_{0u/g} |^2$ for the $0 \leftrightarrow 1$ transition is close to unity, while that for $0 \leftrightarrow 2$, namely $|\langle 0_{\text{OO}} |_{2g} \langle 0_{\text{OO}} \rangle_{0g} |^2$, is much less.

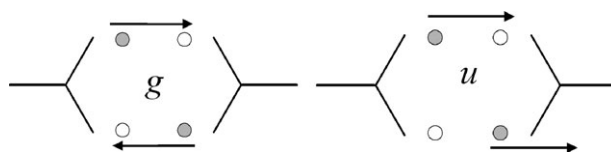


Fig. 8 Schematic representation of the displacement vectors for pseudoparticles in the stretching excited states. Grey and opened circles correspond to occupied and unoccupied sites, respectively, in the ground state.

Upon visual examination of Fig. 7 we estimate that this factor is roughly $|0.5|^2$, hence $\mathcal{I}_{00\leftrightarrow 02}/\mathcal{I}_{00\leftrightarrow 12} \approx 6$. The weak transition moment for the combination band is therefore counterbalanced by the favorable Franck–Condon factor. This is in reasonable agreement with the observed intensity ratios of ≈ 5 for $\mathcal{I}_{2603}/\mathcal{I}_{2781}$ and $\mathcal{I}_{2602}/\mathcal{I}_{2773}$ in Fig. 2 and 3, respectively.

Furthermore, the double minimum potential offers a tentative explanation for the dramatic contrast between the sharp Raman bands and the broad infrared profiles that cannot be attributed to nonadiabatic coupling terms, or any alternative coupling terms. In contrast to the totally symmetric oscillations observed in Raman, the infrared active antisymmetric displacements with large amplitudes (Fig. 8 *u*) are incompatible with stationary motions of pseudoprotons. Excited states are therefore overdamped and relax down along the upper $O\cdots O$ adiabatic potential. Homogeneously broadened profiles can be thought of as complicated interference patterns including, eventually, interaction with multiphonons.³⁸

The same conclusions hold for νOD . The Raman bands are much narrower than their infrared counterparts. Moreover, the narrowing of the infrared profile, compared to νOH , accords with a decrease of the upper adiabatic potential slope for $\nu O\cdots O$ upon deuteration.

4.2. Nonlocal tunnelling states

Dynamical models for stochastic interconversion of uncorrelated dimers^{10,12–14,21,30,31} accord with our intuition based on the everyday classical world. A proton is either here or there and a dimer is in form **T1** or **T2**. However, this view is in conflict with some observations.

With neutron diffraction we probe space and time averaged probability densities at crystal sites, thanks to the translational symmetry of the lattice. For a random mixture of tautomers, say $\alpha^2\mathbf{T1} + (1 - \alpha^2)\mathbf{T2}$, spatial correlations should be partially destroyed and a significant amount of the coherent scattering should collapse into off-Bragg peak diffuse scattering. Well-studied examples, like ice Ih or C₆₀ and many others, are presented in ref. 41. A decrease of the total probability density for protons, compared to that anticipated from the chemical formula, should be observed. At room temperature, $\alpha^2 \approx 0.5$, the average scattering length for protons should be reduced by a factor of ≈ 2 .⁴¹

This is at variance with experiments. The sum of probability densities for protons is equal to unity and temperature independent.⁸ Clearly, interconversion does not destroy the spatial coherence and there is no evidence for stochastic disorder. Moreover, the center of symmetry for dimers is preserved at any temperature. The crystal is therefore a mixture of two centrosymmetric structures: **I** composed of **T1**, prevailing at low temperatures, and the thermally activated configuration **II** composed of **T2**. (From Bragg diffraction it is not possible to conclude whether the mixture is a superposition state.)

With infrared and Raman we probe dynamics at the Brillouin-zone center corresponding to in-phase oscillations of the unit cells throughout the crystal. A straightforward consequence of the uncertainty principle is that only spatially extended states, on the scale of the incident wavelength, are

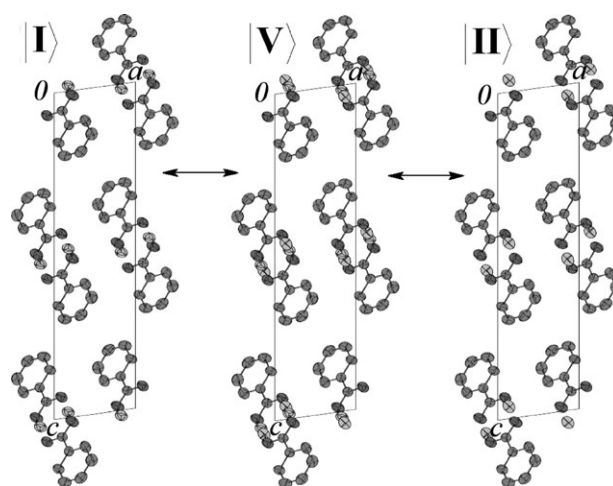


Fig. 9 Schematic representation of the single-pseudoparticle two-step interconversion mechanism, projected onto the (*a*, *c*) plane. In the intermediate virtual state with twofold degeneracy all sites are equally occupied. For the sake of clarity, H atoms bound to the benzoic ring are omitted.

observables. Normal coordinates (2), pseudoparticles and potential functions are therefore extended on the same scale.

The $|0\rangle$ and $|1\rangle$ states of the double minimum potentials are largely localized (to order ϵ) in each well. The ground state is representative of **I** (to order ϵ) and can be thought of as a vector state **|I>** (Fig. 9). State $|1\rangle$ corresponding to the transfer of a pseudoproton is sketched as **|V>** in Fig. 9. All proton sites are equally occupied. This state is twofold degenerate. Finally, the crystal configuration **II** corresponding to the transfer of \mathcal{P}_g and \mathcal{P}_u can be viewed as an extended state **|II>** at $2 \times h\nu_{01}$. **|I>**, **|V>** and **|II>** are “single-pseudoparticle” states, for which each pseudoparticle is evenly distributed over a macroscopic number of sites (\mathcal{N}) and the occupation number per site is $(2\mathcal{N})^{-1}$ for \mathcal{P}_g or \mathcal{P}_u .

|V> is an intermediate in the interconversion process. The **|I>** \leftrightarrow **|V>** and **|V>** \leftrightarrow **|II>** transitions are first order, while the direct transition **|I>** \leftrightarrow **|II>** is second-order. A similar intermediate state, reported for KHCO₃,²⁴ was termed “virtual” because its population does not obey Boltzmann’s law. However, as the $|0\rangle \leftrightarrow |1\rangle$ transition is effectively observed, one can say that this state does not exist if it is not measured/observed.

Quantum interferences have revealed that KHCO₃ in thermal equilibrium is a superposition of macroscopically entangled states. In principle, there is no objection to apply the same theoretical framework to the benzoic acid crystal, but this would be rather formal as long as there is no direct evidence for quantum interferences. The dynamical model elaborated for benzoic acid in a previous work¹⁵ suggests that the interconversion rate is consistent with quantum beats arising from superposition states, but this is a rather circumstantial evidence.

4.3. Isotopic mixtures

The Raman spectrum in Fig. 4 conveys a dramatic information: the bands at 2604 and 2637 cm⁻¹ supposedly due to

mixed (HD) dimers are virtually at the same frequencies as those for BA- h_6 in Fig. 2. Similarly, the infrared profile is almost unchanged. We suppose the bands at 2781 and 2910 cm^{-1} for BA- h_6 (see Table 1) should be also unaffected but, presumably, they are too weak to be observed.

Beyond the straightforward evidence for the lack of Davydov splitting, it is tempting to conclude that protons diluted in the deuteron matrix experience the same double minimum potential as those in the totally hydrogenated derivative. This suggests that proton dynamics are still those of nonlocal centrosymmetric pseudoparticles in a mixture of independent hydrogenated and deuterated sublattices.

Such nonlocal dynamics accord with the continuous change of the NMR interconversion rate as a function of the ratio $\rho = [\text{D}]/([\text{H}] + [\text{D}])$.⁴² However, these measurements have been questioned by another group.²¹ Our results are strong incentives to pursue these experiments.

4.4. Adiabatic pairwise transfer

Upon the assumption that broad infrared profiles arise from double minimum potentials, the sharp infrared-active zero-phonon bands suggest, by contrast, that protons in the relaxed excited states experience single minimum potentials. This is quite possible because these states correspond to a dramatic shortening of $R_{\text{O}\cdots\text{O}}$. Since a symmetric single-minimum is anticipated for $R_{\text{O}\cdots\text{O}} \approx 2.45 \text{ \AA}$,³³ the shortening should be of $\approx 0.15 \text{ \AA}$. This is in qualitative agreement with the weak intensities for zero-phonon bands, due to the small overlap of the $\nu\text{O}\cdots\text{O}$ wave functions. The $\nu\text{O}\cdots\text{O}$ transition in the upper potential, namely $|0g\rangle|2u\rangle|0_{\text{OO}}\rangle_{0g}|0_{\text{OO}}\rangle_{2u} \leftrightarrow |0g\rangle|2u\rangle|0_{\text{OO}}\rangle_{0g}|1_{\text{OO}}\rangle_{2u}$, at $\approx 800 \text{ cm}^{-1}$ provides support to a dramatic stiffening of the $\text{O}\cdots\text{O}$ bond, a normal consequence of its reduced length. Moreover, the νOH transition $|0g\rangle|2u\rangle|0_{\text{OO}}\rangle_{0g}|0_{\text{OO}}\rangle_{2u} \leftrightarrow |0g\rangle|3u\rangle|0_{\text{OO}}\rangle_{0g}|0_{\text{OO}}\rangle_{3u}$ at $\approx 120 \text{ cm}^{-1}$ is in line with the very flat νOH potential expected for short symmetric hydrogen bonds.

The zero-phonon states $|z\rangle$ can be therefore regarded as extended transition states for the interconversion mechanism depicted in Fig. 10. In contrast to “vertical” transitions between tunnelling states (Fig. 9), the electronic structure should follow adiabatically the pairwise proton transfer, through the shortening of $R_{\text{O}\cdots\text{O}}$. Dimers in the transition state could be D_{2h} but there is no direct evidence for this symmetry. Compared to the scheme in Fig. 9, the longer reaction path mixing r and R coordinates, the much heavier effective mass due to large displacements of heavy atoms and the energy difference $2h\nu_{01}$ between the initial and final states concur to cancel out tunnelling. The through-barrier interconversion can be ignored.

The proton transfer rate should be roughly proportional to the thermal population of the zero-phonon states, to the frequency of the low frequency mode (over barrier crossing) and to the statistical distribution of tautomers:

$$k_{\text{I}\rightarrow\text{II}} \sim \frac{1}{2} h\nu_{00} \exp\left(-h \frac{\nu_{z\rho} + 2\nu_{01}}{kT}\right). \quad (4)$$

This gives $\sim 10^8 \text{ s}^{-1}$ at 300 K and $\sim 10^{-2} \text{ s}^{-1}$ at 100 K. This process has no significant impact to the measured rates of

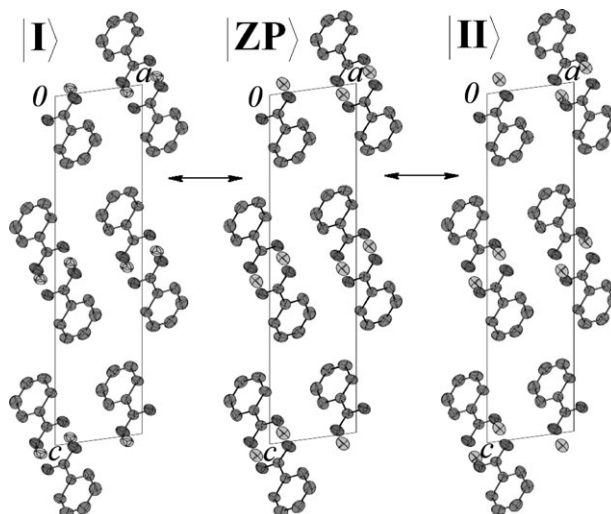


Fig. 10 Schematic representation of the adiabatic pairwise transfer, projected onto the (a, c) plane. In the intermediate zero-phonon state protons are close to the $\text{O}\cdots\text{O}$ centers. For the sake of clarity, H atoms bound to the benzoic ring are omitted.

$\sim 10^{11}$ and $\sim 10^9 \text{ s}^{-1}$ at these temperatures. In addition, the weak frequency shift of the zero-phonon bands upon deuteration contrasts with the large isotope effect on the observed transfer rate.

4.5. Comparison with theoretical works

Among numerous theoretical investigations of benzoic acid dimers we shall consider only the most recent state-of-the-art works.^{19,20} They have in common a semiclassical approach to correlated pair dynamics across a subspace of the Born–Oppenheimer potential energy surface.

According to Tautermann *et al.*,¹⁹ the optimal tunnelling path is rather close to the minimum-energy path and quite different from the straight line between the minima. The transition state with $R_{\text{O}\cdots\text{O}} = 2.42 \text{ \AA}$ is consistent with a symmetric hydrogen bond and a flat single minimum potential for νOH . The computed barrier of $\approx 2500 \text{ cm}^{-1}$, if we subtract the zero-point energy of $\approx 800 \text{ cm}^{-1}$, compares quite nicely with the zero-phonon transitions observed at $\approx 1800 \text{ cm}^{-1}$. The effective tunnelling mass is rather large and the splitting of $\sim 10^{-3} \text{ cm}^{-1}$ for the isolated dimer is insignificant compared to the potential asymmetry in the crystal.

Smedarchina *et al.*²⁰ have determined extreme tunnelling trajectories with the approximate instanton method. The potential barrier was evaluated with the heavy atoms fixed in the equilibrium configuration, which sounds similar to the adiabatic separation of proton/deuteron dynamics. After renormalization including transverse modes, the effective barriers of 5520 and 4380 cm^{-1} for HH and DD pairs are quite close to those given in Table 2. However, the calculated tunnel splitting of $\approx 0.06 \text{ cm}^{-1}$ for HH pairs is two orders of magnitude less than $h\nu_{0r}$ in Table 2.

We suspect this discrepancy to be a consequence of an inappropriate dynamical model for the pair treated as a semiclassical rigid entity. Extrapolating our potential, the

splitting of $\approx 0.06 \text{ cm}^{-1}$ suggests an effective mass in the range 3–4 amu, in line with the large contribution of O \cdots O coordinates to the tunnelling mode depicted in Fig. 3 of ref. 20. We speculate that if proton dynamics were treated as quantum pseudoparticles adiabatically separated from heavy atoms, then the tunnel splitting should increase by about two orders of magnitude, and could be consistent with our own estimates (Table 2). It could be thus possible to establish excellent contact between experiments and first-principles calculations.

If it were the case, this would show that, quite surprisingly, nonlocal proton dynamics, purely quantum in nature, are monitored by the Born–Oppenheimer potential energy surface calculated with classical protons. In fact, these calculations are based upon correlated displacements of rigid proton pairs, which preserve the center of symmetry, although there is no strong proton–proton interaction. This can be thought of as a semiclassical approach to nonlocal dynamics, which may explain the consistency with observed quantum dynamics.

5. Experimental

Sample preparation as well as infrared and Raman measurements were described in ref. 15. The fully hydrogenated (BA- h_6) and ring deuterated (BA- d_5h) 98%, Euriso-Top S. A.) benzoic acids were commercial products. They were sublimated. The (BA- h_5d) derivative was obtained after three exchanges with commercial methanol CH₃OD (98%). The ratio of the integrated intensities over the ν OH and ν OD Raman bands gives $\approx 15\%$ of residual OH groups.

The Raman spectra were obtained with a DILOR XY triple monochromator equipped with an Ar⁺ laser emitting at 4880 Å. The spectral resolution was $\approx 2 \text{ cm}^{-1}$. Powdered samples were sealed in capillary glass tubes and then loaded into a liquid helium cryostat. The temperature was measured with a thermometer just above the sample.

Energy levels and wave functions were calculated with the variational method¹⁵ utilizing a basis sets of 40 harmonic wave functions with fundamental frequency $\hbar\omega_0$. For each potential function this parameter is optimized so as to obtain the lowest energy for the ground state.

6. Conclusion

Raman spectra of the ν OH/OD modes of benzoic acid crystals demonstrate long-life stationary extended states and adiabatic separation from heavy atom dynamics. Coupling terms at the Born–Oppenheimer level are embedded in adiabatic potentials and H/D dynamics are those of bare particles. In addition, intradimer and interdimer coupling terms are strictly negligible.

Our tentative assignment scheme suggests that the quasi-symmetric double-minimum potential for ν OH/OD is the leading band shaping factor. The ground state splitting is observed as a combination with the $|0\rangle \leftrightarrow |2\rangle$ transition, thanks to large overlap of the ν O \cdots O wave functions in the lower states. Potential functions are then totally determined. The tunnelling mass is 1(2) amu for H(D) atoms. Furthermore, the double minimum potential may account for the dramatic

contrast between broad infrared profiles and sharp Raman bands.

The double-well potentials are temperature independent. Incoherent tunnelling, stochastic disorder, coupling with phonons, symmetrization of the double minimum, over-barrier jumping and transition from quantal to classical regime are not supported by any evidence. Models based upon these dynamics should be questioned.

As there is no stochastic disorder arising from the thermally activated interconversion, and no coupling between protons (deuterons), the local transfer of either single H/D atoms, or correlated pairs, can be ruled out. Consequently, we introduce extended pseudoparticle states preserving the crystal symmetry and periodicity. This leads to a two-step interconversion mechanism between structure states **I**) and **II**) through the intermediate state **V**). In this latter state, pseudoprotons are evenly distributed over all sites.

An alternative interconversion route goes through extended zero-phonon states. The intermediate configuration with very short O \cdots O distances corresponds to single-minimum hydrogen bonds, possibly symmetrical. The estimated interconversion rate is negligible by orders of magnitude compared to measurements.

The excellent agreement between potentials derived from experiments and those computed with first-principles methods suggests that the Born–Oppenheimer potential energy surfaces for an isolated dimer and for the crystal are similar. It is thus confirmed that interdimer coupling terms are negligible. The potential asymmetry in the crystal can be tentatively attributed to a temperature independent static field.

References

- 1 L. Pauling, *The nature of the chemical bond*, Cornell University Press, Ithaca, New York, 1960.
- 2 S. N. Vinogradov and R. H. Linnell, *Hydrogen Bonding*, Van Nostrand-Reinhold, New York, 1971.
- 3 P. Schuster, G. Zundel and C. Sandorfy, *The hydrogen bond. Recent developments in theory and experiments*, Vol. I, II and III, North-Holland Pub. Co., Amsterdam, 1976.
- 4 P. Schuster, *Hydrogen Bonds*, Springer-Verlag, Berlin, 1984.
- 5 G. A. Jeffrey and W. Saenger, *Hydrogen Bonding in Biological Structures*, Springer-Verlag, Berlin, 1991.
- 6 C. L. Perrin and J. B. Nielson, *Annu. Rev. Phys. Chem.*, 1997, **48**, 511.
- 7 S. Scheiner, *Hydrogen Bonding: A Theoretical Perspective*, Oxford University Press, Oxford, 1997.
- 8 C. C. Wilson, N. Shankland and A. J. Florence, *Chem. Phys. Lett.*, 1996, **253**, 103–107.
- 9 S. Nagaoka, T. Terao, F. Imashiro, A. Saika, N. Hirota and S. Hayashi, *Chem. Phys. Lett.*, 1981, **80**(3), 580–584.
- 10 B. H. Meier, F. Graf and R. R. Ernst, *J. Chem. Phys.*, 1982, **76**(2), 767–774.
- 11 S. Nagaoka, T. Terao, F. Imashiro, A. Saika, N. Hirota and S. Hayashi, *J. Chem. Phys.*, 1983, **79**(10), 4694–4703.
- 12 A. Gough, M. M. I. Haq and J. A. S. Smith, *Chem. Phys. Lett.*, 1985, **117**(4), 389–363.
- 13 A. Stöckli, B. H. Meier, R. Kreis, R. Meyer and R. R. Ernst, *J. Chem. Phys.*, 1990, **93**(3), 1502–1520.
- 14 J. L. Skinner and H. P. Trommsdorff, *J. Chem. Phys.*, 1988, **89**, 897–907.
- 15 F. Fillaux, M.-H. Limage and F. Romain, *Chem. Phys.*, 2002, **276**, 181–210.
- 16 M. R. Johnson and H. P. Trommsdorff, *Chem. Phys. Lett.*, 2002, **364**, 34–38.

-
- 17 G. M. Florio, T. S. Zwier, E. M. Myshakin, K. D. Jordan and E. L. Siebert, III, *J. Chem. Phys.*, 2003, **118**(4), 1735–1746.
- 18 M. Boczar, K. Szczponek, M. J. Wójcik and C. Paluszkiwicz, *J. Mol. Struct.*, 2004, **700**, 39–48.
- 19 C. S. Tautermann, A. F. Voegelé and K. R. Liedl, *J. Chem. Phys.*, 2004, **120**(2), 631–637.
- 20 Z. Smedarchina, A. Fernandez-Ramos and W. Siebrand, *J. Chem. Phys.*, 2005, **122**, 134309.
- 21 Q. Xue, A. J. Horsewill, M. R. Johnson and H. P. Trommsdorff, *J. Chem. Phys.*, 2004, **120**(23), 11107–11119.
- 22 O. Henri-Rousseau and P. Blaise, in *Advances in Chemical Physics*, ed. I. Prigogine and S. A. Rice, Wiley, Hoboken, NJ, 1998, vol. 103, p. 1.
- 23 L. Colombo and K. Furic, *Spectrochim. Acta, Part A*, 1971, **27**, 1773–1784.
- 24 F. Fillaux, A. Cousson and M. J. Gutmann, *J. Phys.: Condens. Matter*, 2006, in press.
- 25 C. C. Wilson, N. Shankland and A. J. Florence, *J. Chem. Soc., Faraday Trans.*, 1996, **92**, 5051.
- 26 J. E. Bertie, K. H. Michaelian, H. H. Eysel and D. Hager, *J. Chem. Phys.*, 1986, **85**(9), 4779–4789.
- 27 J. C. Evans, *Spectrochim. Acta*, 1960, **16**, 994.
- 28 J. C. Evans, *Spectrochim. Acta*, 1962, **18**, 507.
- 29 U. Fano, *Nuovo Cimento*, 1935, **12**, 156.
- 30 A. J. Horsewill, A. Ikram and I. B. I. Tomsah, *Mol. Phys.*, 1995, **84**(6), 1257–1272.
- 31 D. F. Brougham, A. J. Horsewill and R. I. Jenkinson, *Chem. Phys. Lett.*, 1997, **272**, 69–74.
- 32 C. Cohen-Tannoudji, B. Diu and F. Laloë, *Mécanique Quantique*, Hermann, Paris, France, 1977.
- 33 A. Novak, *Struct. Bonding*, 1974, **18**, 177–216.
- 34 B. I. Stepanov, *Nature*, 1946, **157**, 808.
- 35 A. Witkowski, *J. Chem. Phys.*, 1967, **47**(9), 3645–3648.
- 36 Y. Maréchal and A. Witkowski, *J. Chem. Phys.*, 1968, **48**(6), 3697–3705.
- 37 S. F. Fischer, G. L. Hofacker and M. A. Ratner, *J. Chem. Phys.*, 1970, **52**(4), 1934–1947.
- 38 F. Fillaux, *Chem. Phys.*, 1983, **74**, 405.
- 39 F. Fillaux, A. Cousson and M. J. Gutmann, *J. Mol. Struct.*, 2006, in press.
- 40 F. Fillaux, *Chem. Phys. Lett.*, 2005, **408**, 302–306.
- 41 V. M. Niold and D. A. Keen, *Diffuse neutron scattering from crystalline materials. Vol. 14 of Oxford series on neutron scattering in condensed matter*, Clarendon Press, Oxford, 2001.
- 42 S. Takeda and A. Tsuzuminati, *Magn. Reson. Chem.*, 2001, **39**, S44–S49.